Received: 8 April 2020 | Revised: 1 July 2021 | Accepted: 18 August 2021

DOI: 10.1002/stc.2842

RESEARCH ARTICLE

WILEY

Enhancement of chromatographic spectral technique applied to a high-speed train

Alejandro Bustos[1] | **Higinio Rubio**[1] | **Cristina Castejon**[1] | **Juan Carlos Garcia-Prada**[2]

[1]MAQLAB Research Group, Department of Mechanical Engineering, University Carlos III of Madrid, Madrid, Spain

[2]MAQLAB Research Group, Department of Mechanics, National Distance Education University, Madrid, Spain

Correspondence
Alejandro Bustos, MAQLAB Research Group, Department of Mechanical Engineering, Universidad Carlos III de Madrid, Av. de la Universidad, 30, 28911 Leganes, Madrid, Spain.
Email: albustos@ing.uc3m.es

Funding information
UNED, Grant/Award Number: 2021-MEC-25; Spanish Government: MAQ-STATUS project, Grant/Award Number: DPI2015-69325-C2-1-R

Summary

High-speed rail is a key player in people's mobility thanks to its speed and high safety standards. These high safety standards are supported by extensive maintenance (of both rolling stock and track) that applies the latest nondestructive and monitoring techniques. In that context, this work presents the enhanced graphical representation of state configurations (EGRSC) and enhanced chromogram of bands of frequency (ECBF) methods, which are the evolution of the graphical representation of State configurations and chromogram of bands of frequency techniques. A clearer nomenclature is defined for the configuration states of the EGRSC. The ECBF introduces a new variable threshold that allows discarding frequency regions with small power variations and a new color palette. These methods are used in the vibratory study of an in-service high-speed train to identify the operating condition of the train. To conduct that task, a set of accelerometers is installed on the axle box of a trailer axle of the train. Accelerometers are oriented into the three space directions: longitudinal, lateral, and vertical. Vibration signals are taken during the normal operation of the train and transmitted to and stored on a remote database. Vibration measures are collected before and after a major maintenance operation. The application of EGRSC and ECBF allows collecting information from thousands of vibration signals and to display that information intuitively and understandably. The analysis of EGRSC and ECBF results allows identifying several frequency regions with significant spectral power variations that are common to the three vibration directions studied. These patterns should be taken as a reference for future maintenance actions. Any unexpected behavior of these frequency regions would indicate the presence of a fault.

KEYWORDS

ECBF, EGRSC, high-speed rail, maintenance

1 | INTRODUCTION

The first high-speed line was opened in 1964 and joined the cities of Tokyo and Osaka in Japan. Since then, many countries around the world have opened high-speed lines with exponential growth in recent years. According to the International Union of Railways, more than 46,000 km of high-speed lines are in operation currently, and another 44,000 km are planned for the next years.[1] In 2017, high-speed trains (HSTs) transported 844.8 billion passenger-km.[2]

In order to keep passengers safe, extensive maintenance is required both in rolling stock and infrastructure. Even then, catastrophic accidents can occur due to maintenance-related failures. For example, we can cite the disaster of Eschede (Germany) in 1998, in which the ICE 884 train derailed due to a broken wheel and killed 101 persons.[3] Another example is the Wenzhou (China) accident in 2011, in which two HSTs collided due to "serious design flaws" in the signaling and control systems and poor track maintenance. Forty people died as a result of that collision.[4]

Multiple studies are carried out to improve rail maintenance and, therefore, reduce the number of accidents and their consequences.

Usually, inspection techniques like ultrasonic testing, electromagnetic methods, acoustic emission, temperature measurement, or strain gauges are applied to monitor the condition of rolling stock and tracks. Several papers exposing the results of applying those techniques (or improved versions of them) can be found in the scientific literature.[5–16] However, most of these techniques require specific equipment that makes their implementation on in-service rolling stock difficult.

Vibration analysis has advantages over other techniques because it notices changes immediately and allows permanent and intermittent monitoring, and lots of signal processing techniques can be used.[17]

Many works focus on the vibration analysis of rail wheelsets, as this is a crucial mechanical system to guarantee the safety of the whole vehicle. Frequently, the key mechanical components studied are faulty bearings within the transmission system[18] and the axle box,[19,20] the existence of wheel flats,[21–23] and axle cracks.[24–28] Generally, this kind of researches is carried out in laboratory conditions and combining numerical models with actual vibration measurements.

However, studies carried out with in-service rolling stock are not so common. Papaelias et al.[29] suggested a method based on high-frequency acoustic emission and vibration analysis to monitor rolling stock. They tested a freight wagon with faulty bearings first, and a second test was carried out by monitoring an in-service train with wheel defects. Bustos et al.[30] studied the operating condition of an in-service HST through the empirical mode decomposition (EMD). Vibration signals were measured from the axle box of a trailer bogie for several months. Ham[31] presented vibration data collected from a motor bogie of the Korean HST, but only two journeys were processed. Wang et al.[32] analyzed the axle box vibration of in-service HST with the aim of extending the wheel reprofiling interval. The main objective of this work was to establish a wear limit that optimizes reprofiling operations. Gasparetto et al.[33] monitored the running stability of a high-speed railway bogie to detect and resolve different faults that may occur in the bogie components, as the increased conicity due to wheel wear and the degradation of yaw dampers. Zhang et al.[34] and Wang et al.[35] applied Bayesian forecasting to vibration and strain measurements obtained from HSTs at speeds up to 250 km/h. The studies carried out by these authors showed that the proposed methods can detect the effects that wheel reprofiling has not only on the bogie but also on the passenger's comfort.

The study of defects in railway systems generates large amounts of data that require the use of complex models and/or artificial intelligence techniques for data processing. However, these techniques need well-defined input data that are not always available.

This work studies the vibratory behavior of a HST bogie before and after a major maintenance operation to define critical frequency regions that allow identifying faults during the normal train operation. To that end, a HST is equipped with an on-board measurement system that acquires and transmits vibration signals without interrupting the normal operation of the train. The vibration signals are processed by using improved versions of the graphical representation of state configurations (GRSC) and chromogram of bands of frequency (CBF) techniques that were introduced in Bustos et al.[36]

These new techniques are called enhanced graphical representation of state configurations (EGRSC) and enhanced chromogram of bands of frequency (ECBF) and try to overcome some limitations of the original methods. First, the nomenclature of the GRSC used the same letters for defining the operating states of the system and the available configurations, which could be confusing. To avoid this, a clearer nomenclature of the configuration states will be defined for the EGRSC. Consequently, it is impossible to take the operating states of the system for the configuration states and vice versa now. Second, the color scale of the CBF will be modified, and a new variable threshold will be added.

The original method does not take into account relative power variations between the operating states, which could lead users to focus on frequency regions whose power variation is minor. The new threshold is intended to discard frequency regions with small power variations and to emphasize the frequency regions that undergo significant power variations.

The structure of the paper is as follows. The applied techniques are described in Section 2. Then, the measurement system is briefly depicted and the measurement conditions are described in Section 3. The fourth section discusses the results of applying the EGRSC and ECBF techniques, and the last section states the conclusions.

2 | METHODS

As stated in Bustos et al.,[36] the basis of the GRSC and the CBF is the computation of the frequency spectrum of a signal (or the average spectrum of several signals). Then, this frequency spectrum is divided into several frequency bands or power packets by applying the multilevel analysis (MLA). Figure 1 illustrates the logic of the decomposition process: the initial spectrum is split into two halves, and each half is split again into two halves, and so on. Thus, the initial spectrum is divided into 2^k bands, being k the decomposition level.

The decomposition algorithm can be summarized in Equation 1, where i is the index of the signal's array of data, j is the packet's number for a decomposition level k, k is the decomposition level, N is the number of points of the signal, $Sx(i)$ is the value of the power spectral density (PSD) at index i, and $P(k,j)$ is the power of the packet j for the decomposition level k.

The algorithm definition implies that the value of k must be such that the result 2^k will be always less or equal to the number of points N in the vibration signal—that is to say, $2^k \leq N$, and k results in an integer.

$$P(k,j) = \sum_{j=1}^{j=2^k} \sum_{i=\frac{N}{2^k}(j-1)+1}^{i=\frac{N}{2^k}j} S_x(i). \tag{1}$$

GRSC and CBF methods are based on the typical deterioration time curve for machinery (see Figure 2), the well-known "bathtub" curve. Three periods can be distinguished in these curves.[37,38] The first period corresponds to the running-in of the machine, in which young failures may occur.

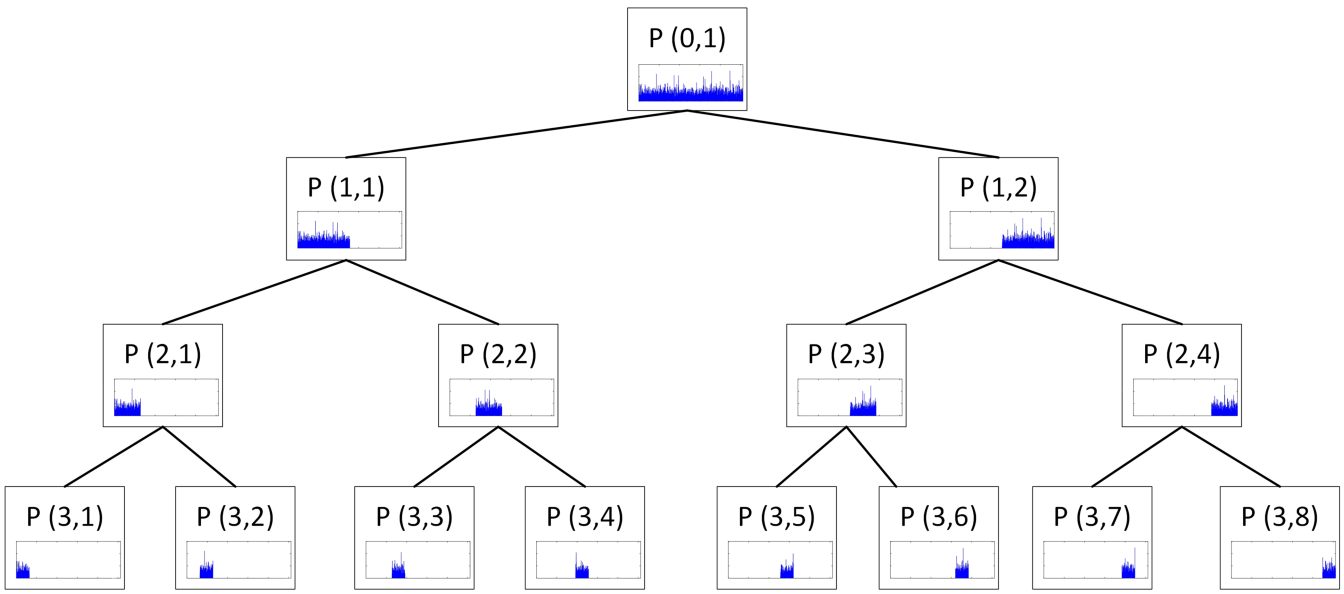

FIGURE 1 Scheme of the decomposition process (MLA)

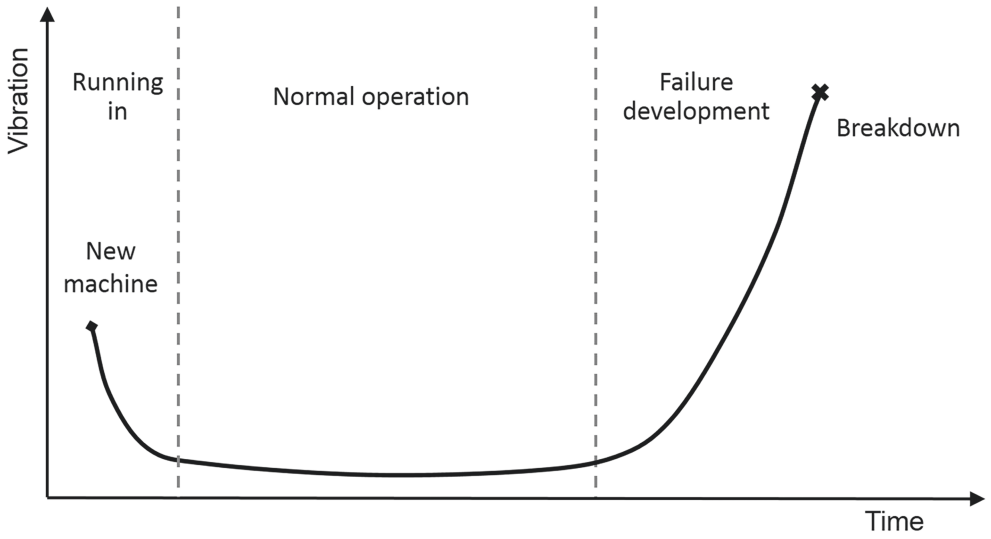

FIGURE 2 Typical deterioration curve for machinery

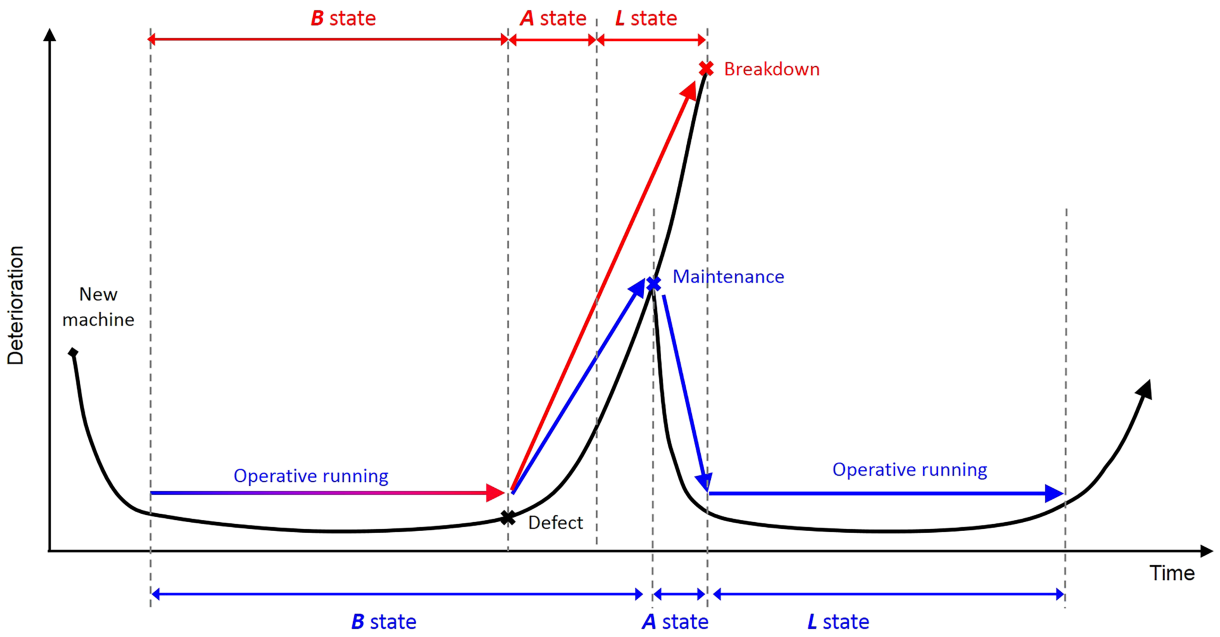

FIGURE 3 Operating states for maintenance action (in blue) and operating states for deterioration study (in red)

The second period is the normal operation of the machine, in which the deterioration level increases very slowly due to normal wear. The last period corresponds to a fast increase as the machine approaches breakdown.

Keeping this curve in mind, three operating states are established taking as reference a significant milestone, which can be a maintenance task or the substitution of a relevant element of the rolling stock. These states do not match the previous periods necessarily. According to that noteworthy milestone, we can define the operating states B (Before), A (After), and L (Later). Operating state B will collect all the measurements taken before the event. Operating state A will compile the measurements taken just after the event, i.e., the first operating moments of the system after that significant event. The operating state L will group the measurements taken after the operating state A.

Figure 3 represents two scenarios over the "bathtub" curve. The first scenario is the study of a maintenance action in a machine (in blue). The second scenario is the study of a deterioration process up to breakdown (in red). In the maintenance action scenario, the vibration level increases until the machine is repaired (all this period is the operating state B). Next, the vibration level suffers a rapid descend (operating state A) and then returns to the normal operation

level (state L). In the deterioration scenario, the machine runs at its normal vibration level (state B) until the initial defect occurs (state A) and the vibration level suffers a rapid increase as the defect size grows (state L).

The EGRSC is a way of summarizing the deterioration curves in a triangle, taking as a parameter the spectral power of the vibration signals. Figure 4 shows the generation of EGRSC. First, the significant event is placed in the time axis (to get a time reference). Then, the average powers of the packets at each operating state are placed in the timeline and represented with the corresponding letter (B, A, or L). These points are linked with straight lines, and a triangle is constructed. The edges of this triangle are coded with different colors. The edge between the operating states B and A is colored in red. The line joining states A and L is colored in green. The edge that joins the operating states B and L is colored in blue. The color code of the edges makes the identification of the configuration easier in the case two operating states were too close.

The naming code developed in Bustos et al.[36] is improved, so the identification of the possible triangle configurations is easier now. The three-letter structure ("xxx") is kept. The first letter corresponds to the red line, the second letter corresponds to the green line, and the third letter corresponds to the blue line as in the original method. However, the options are just "d" (down, for negative slopes) and "u" (up, for positive slopes) now, instead of "B," "b," "A," "a," "L," and "l" that were available in the original method. According to the shape of the triangle and combining the slopes of the straight lines, we can establish six "dud" configurations that are exposed in Table 1.

The ECBF compiles all the triangles generated in the EGRSC in one image. A numerical value is assigned to each EGRSC configuration. These numerical values are used in MATLAB® to generate a color map according to the color code shown in Table 1. Cold colors identify the configurations that start with "d." That is to say, those configurations

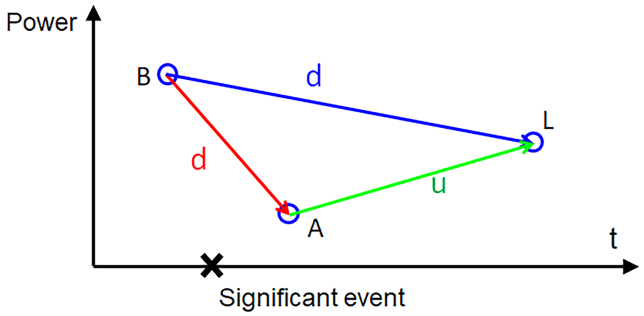

FIGURE 4 Generation of EGRSC

TABLE 1 Color coding of the possible configurations

Configuration	Color	Shape
ddd		
dud		
ddu		
duu		
udd		
uud		
udu		
uuu		

where the spectral power is reduced between the operating states B and A. Warm colors relate to the configurations that start with "u." That is to say, those configurations where the spectral power is increased between the operating states B and A. Then, a color map that associates the frequency, the frequency bandwidth of the power packets, the decomposition level, and the color code is plotted.

The evolution of the original CBF into ECBF implies that the color of the configuration is set to white if the difference between the spectral powers of operating states B and A, and B and L is within a specific threshold. For example, if the threshold value is set to 10%, white will be used to plot all configurations (frequency regions or packet) whose differential spectral powers between operating states B and A, and B and L are lower than 10%. Naturally, the threshold value can be established as desired.

The EGRSC configuration and the color vary according to the nature of the process studied. For example, if the deterioration of a cracked axle is studied, "udd," "udu," "uuu," and warm colors will represent the expected behavior of the system, namely, an increase of the spectral power after the defect apparition (see Figure 3). However, if a repair is studied, "ddd," "dud," "duu," and cold colors should represent the expected behavior of the system. That is, a vibration reduction after the maintenance and a slow growth later (see Figure 3).

3 | SYSTEM

Vibration signals are recorded by a measurement system installed on a HST. This system is composed of three uniaxial accelerometers, a speedometer, two data acquisition units, a communication module, and a remote database. Vibration and rotating speed measurements are transmitted to the database using the cellular network. Then, data are downloaded from the database and processed on a computer.

The accelerometers are placed on the axle box covers of the trailer axle highlighted in Figure 5. The ICP® accelerometers are oriented to the longitudinal, lateral (or axial), and vertical directions (see Figure 6). The accelerometers were provided by SKF®, model CMSS-RAIL-9100, and their performance characteristics are shown in Table 2. The speedometer is an Axletronic® from SKF®.

The data acquisition units and the communication module are located inside the luggage compartment (see Figure 7). The data acquisition units are IMx-R from SKF®. Each IMx-R is equipped with 20 analogical and four digital input channels and can adjust the gain automatically.

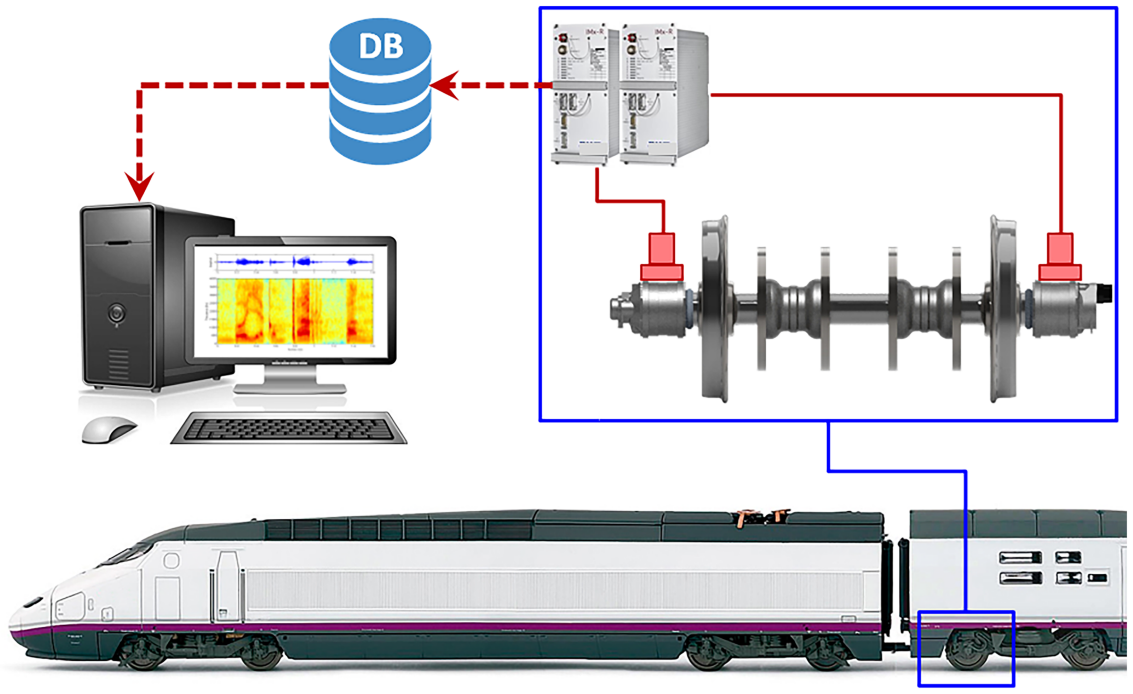

FIGURE 5 Measurement system

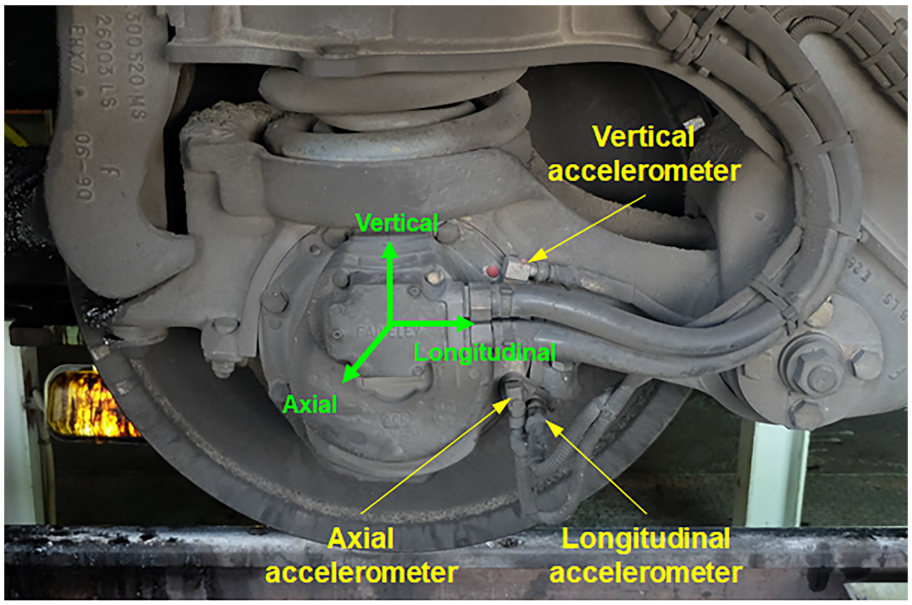

FIGURE 6 Location of the accelerometers on the axle box

TABLE 2 Accelerometer characteristics

Parameter	Value
Sensitivity (±20%)	10.2 mV/(m/s^2)
Acceleration range	±490 m/s^2
Frequency range (±3 dB)	0.52 Hz to 8 kHz
Resonance frequency	25 kHz
Amplitude Linearity	±1%
Transverse sensitivity	≤7%

FIGURE 7 Location of the acquisition system

The system measures and stores the speed every second and is capable to record up to four vibration signals per accelerometer and minute. The parameters for the signal acquisition are shown in Table 3.

To guarantee the uniformity of data, vibration signals are always collected in the same track section and speed during the normal operation. A 150-km section of the high-speed line between Madrid and Seville is selected to perform

TABLE 3 Signal acquisition parameters

Parameter	Value
Sampling frequency (F_s)	5,120 Hz
Acquisition time (per signal)	3.2 s
Number of points N (per signal)	16,384 (2^{14})
Angular speed range for acquisition	75–2,000 rpm
Linear speed range for acquisition	13–347 km/h

TABLE 4 Characteristic frequencies at 270 km/h

Phenomenon	Frequency (Hz)
Axle rotation frequency (F_r)	26.48
Ball pass frequency inner race (*BPFI*)	335.87
Ball pass frequency outer race (*BPFO*)	273.17
Ball spin frequency (*BSF*)	125.36
Fundamental train frequency (*FTF*)	11.89
Sleeper pass frequency (*SPF*)	125
Wheel corrugation frequency	1,500–3,500

the studies in both directions (Madrid to Seville and Seville to Madrid). In this section, the train runs at a steady speed of 270 km/h.

The two wheels of the monitored axle were reprofiled during scheduled maintenance. Signals are analyzed before and after that maintenance action. Three operating states are defined by considering the date on which the vibration signals were collected and the signal processing techniques described above:

- State B: this operating state groups all the vibration data that were collected during the 2 weeks before maintenance works.
- State A: this state groups the vibration data collected the first day the train returned to service after the maintenance works.
- State L: the last operating state groups the vibration data recorded from state A to 1 month after the maintenance works.

During the test campaign, around 4,200 vibration signals were recorded on that section of the Madrid–Seville high-speed line.

They exist several characteristic frequencies that should be known before performing the data analysis. Table 4 shows the actual frequency value of physical phenomena that play a key role in the dynamical behavior of the train. The axle rotation frequency is directly related to the vehicle's speed through the wheel radius. The roller bearing fault frequencies are also computed for defects in the inner ring (ball pass frequency inner race or BPFI), the outer ring (ball pass frequency outer race or BPFO), the rolling element (ball spin frequency or BSF), and the cage (fundamental train frequency or FTF). The sleeper pass frequency (SPF) is computed using Equation 2, where v is the train's speed and λ is the space between sleepers. Significant frequencies due to other phenomena like wheel corrugation are obtained from the literature.[39]

$$SPF = f = \frac{v}{\lambda}. \tag{2}$$

All these values are computed for a speed of 270 km/h (the average travel speed in the analyzed track sector). It must be highlighted the proximity between the BSF of the bearing and the SPF, which could lead to diagnosing a false bearing fault.

4 | RESULTS

This section discusses the results obtained after applying the EGRSC and ECBF methods to the measured vibration signals. The results are presented according to the measurement direction (vertical, longitudinal, and lateral), and the main findings that are common to the three directions are summarized at the end of this section.

Figure 8 shows three vertical vibration signals recorded before (operating state B) and after (operating states A and L) the wheels reprofiling. These signals were recorded in the Madrid–Seville high-speed line at 270 km/h. The PSD of these signals is depicted along with the time signals, and it presents many spectral lines over the whole frequency range. Vibration signals recorded in the longitudinal and lateral directions have a similar appearance.

After removing faulty signals (if any), they are processed by applying EGRSC and ECBF techniques. These techniques are applied per sensor, so the signals are grouped according to the measurement direction (vertical, longitudinal, and lateral) first and to the operating state (before, after, or later) then. After that, the signals of each group are averaged. A decomposition level of $k = 9$ is used for both EGRSC and ECBF. However, to make the reading more dynamic, EGRSC results are presented up to decomposition level $k = 3$ only.

It should be noted that the spectral power of each operating state (B, A, or L) is the average spectral power of all signals recorded in each direction during that period. In addition, spectral power values of operating states B, A, and L are shown on EGRSC ($k = 0$ and $k = 1$) for a better understanding of discarded regions in ECBF.

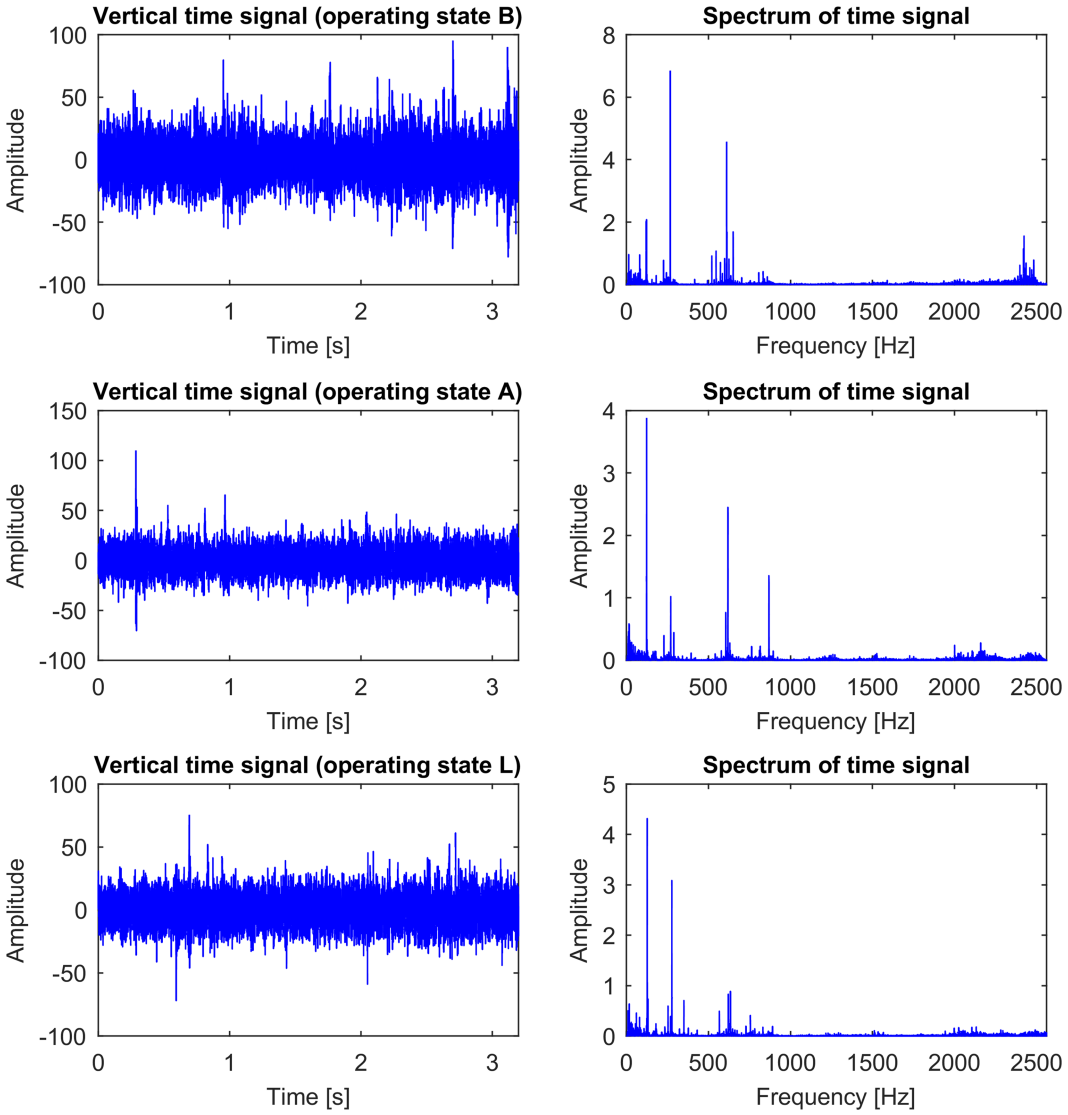

FIGURE 8 Examples of vertical vibration signals and spectra

4.1 | Vertical direction

Figure 9 shows the EGRSC corresponding to the vertical acceleration signals for decomposition levels $k = 0$, $k = 1$, $k = 2$, and $k = 3$.

According to the "ddd" configuration obtained for the decomposition level $k = 0$ (the whole frequency range of the signal), the spectral power of the vertical vibration signals decreases between all the possible operating states configurations. This is one of the three configurations that could be expected after maintenance work (as exposed in Section 2).

The two power packets corresponding to the decomposition level $k = 1$ show different configurations. The first packet displays an "udd" configuration, which indicates the power grows between the B and A states, while it is reduced between operating states A and L and B and L. The second power packet exhibits a "ddd" configuration (the same as level $k = 0$).

The decomposition level $k = 2$ gives four power packets. Three of them present a "ddd" configuration, as the second power packet of decomposition level $k = 1$ does. However, the second power packet (which corresponds to the 640- to 1,280-Hz frequency range) shows an "udu" configuration. This means the spectral power is higher just after the maintenance operation than before.

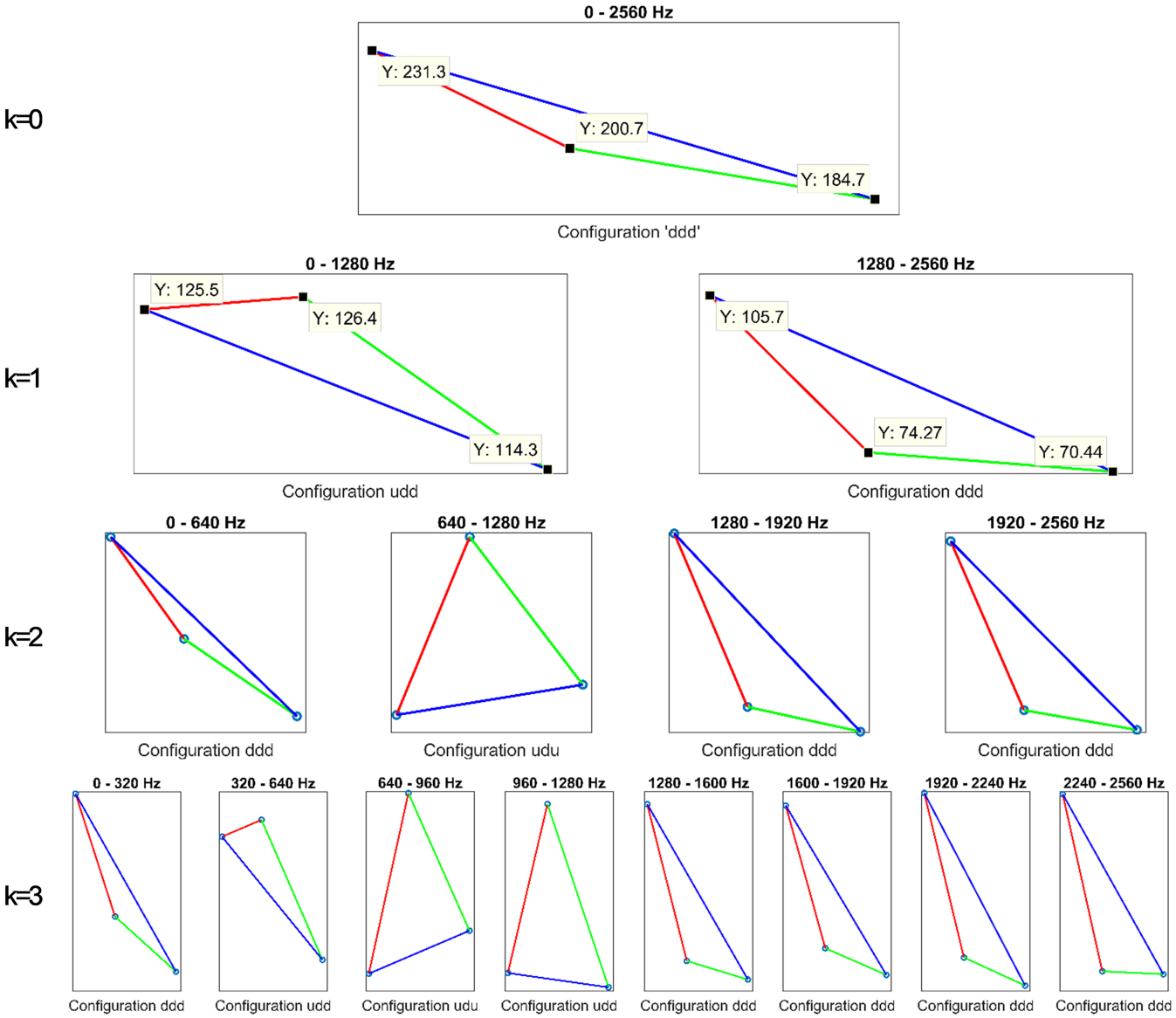

FIGURE 9 EGRSC of vertical accelerations

The eight power packets of the decomposition level $k = 3$ present a variety of configurations. Power packets 1, 5, 6, and 7 show a "ddd" configuration, so the power is always reduced compared to operating state B and also the power of L is reduced compared to A. The second and fourth power packets present an "udd" configuration, so the power is increased between the operating states B and A and reduced at the end of the studied period. The last power packet shows a "dud" configuration. The third power packet shows an "udu" configuration; thus, the spectral power increases after the maintenance operation.

The ECBF corresponding to the accelerations measured in the vertical direction is shown in Figure 10. It compiles the information for decomposition levels from $k = 0$ to $k = 9$. The upper image represents the ECBF with no threshold applied. The middle and lower images show the ECBF with threshold values of 10% and 25%, respectively.

The first row of the ECBF corresponds to decomposition level $k = 0$ and matches the "ddd" configuration of EGRSC, so it is colored in dark blue when a threshold of 0% or 10% is used. However, that row is colored in white when the threshold level of 25% is applied because the power variation between states is lower than that value.

The second row relates to decomposition level $k = 1$, and we find two colors that correspond to the two EGRSC configurations. The first EGRSC configuration is "udd," consequently, and according to Table 1, the color of that bandwidth is orange on the ECBF with a threshold of 0%. However, the ECBFs with thresholds of 10% and 25% show a white section because the variation of the spectral power between the operating states is lower than the established range of 10% and 25%. The bandwidth of the second power packet is painted in the dark blue color corresponding to the "ddd" configuration.

As can be computed from the data shown in Figure 9, power variations for $k = 0$ are -13.2% (B $\rightarrow$ A) and -20.1% (B $\rightarrow$ L). For $k = 1$, we obtain $+0.7\%$ (B $\rightarrow$ A, packet 1), -8.9% (B $\rightarrow$ L, packet 1), -29.7% (B $\rightarrow$ A, packet 2), and -33.3% (B $\rightarrow$ L, packet 2). The relation between the following rows of the ECBF and the EGRSC can be established by following the same procedure.

Based on the results, the ECBF can also be divided into two halves. The right half (between 1,280 and 2,560 Hz) is mainly colored in blue, which is the expected performance of the system after maintenance work (spectral power or vibration is reduced after maintenance). Just small red and orange stripes appear at high decomposition levels around 1,750 Hz.

The left half (0–1,280 Hz) shows a different image: a large bandwidth that spreads from 600 Hz to 1,300 Hz is colored in warm colors. This indicates that the spectral power is increased just after the maintenance operation. Cold colors are the prevailing colors between 0 and 600 Hz, although some orange stripes are also visible.

The small regions discarded when the 10% threshold is applied turn into large excluded areas with a threshold of 25%. The variable threshold allows us to select the frequency regions most sensitive to changes in the system. Specifically, five interesting frequency regions with power reductions are located around 250, 350, 410–580, 1,485–1,680, and 1,800–2,420 Hz. Also, another three frequency regions with power increases are located at 585–780, 825–940, and 1,065–1,220 Hz.

According to literature,[39] the 1,300- to 2,500-Hz frequency region corresponds to the wheel corrugation defect, so the decrease in the spectral power in that frequency region is consistent with the wheels turning. A similar pattern is observed in the power packets that contain the characteristic frequencies of the SPF and the frequencies of the rolling element (BSF), inner (BPFI) and outer race faults (BPFO) of the bearing.

4.2 | Longitudinal direction

The EGRSC obtained from the longitudinal vibrations is shown in Figure 11. Decomposition level $k = 0$ (the whole frequency range of the signal) presents a "dud" configuration, which means a power reduction between the operating states A and B and between A and L, although a power increase is experienced between the operating states B and L. This is one of the expected configurations after a maintenance operation, as stated in Section 2.

The first power packet of decomposition level $k = 1$ shows a "ddd" configuration, whereas the second power packet has a "dud" configuration. This means that the spectral power is reduced between the operating states B and A and between B and L in both power packets. However, the spectral power is decreased between operating states A and L in the first power packet, and it is increased in the second power packet.

Three of the four power packets of the decomposition level $k = 2$ present a "dud" configuration, as could be expected after repair work. However, the second power packet (640–1,280 Hz) shows an "udu" configuration. This configuration means a power increase between the operating states A and B and between A and L and a power reduction between B and L.

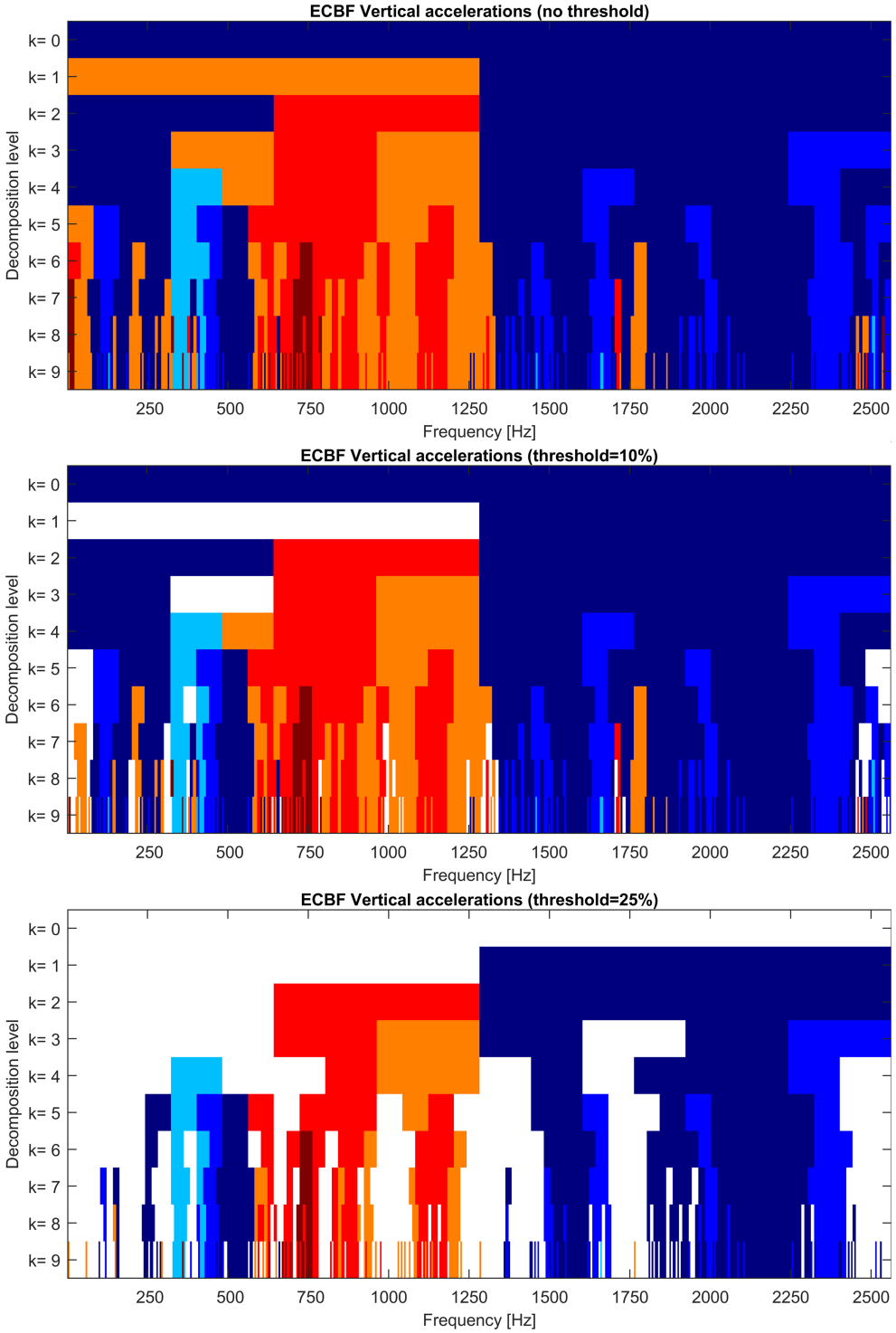

FIGURE 10 ECBF of vertical accelerations with three threshold levels: 0% (up), 10% (middle), and 25% (down)

The decomposition level $k = 3$ offers 8 power packets. Power packets 1, 5, 6, and 7 present the "dud" configuration. The second power packet exhibits a "ddd" configuration, which implies the power is reduced between all the operating states. The third power packet presents an "udu" configuration. The fourth power packet shows an "udd" configuration. So, the spectral power of these two power packets is increased just after maintenance. The power packet 8 presents a "duu" configuration, which means that, although the power is reduced just after the maintenance, the global result is a power increase.

The ECBF corresponding to the accelerations measured in the longitudinal direction is shown in Figure 12. As previously, the ECBF has been plotted using three threshold values: 0% (no threshold), 10% and 25%.

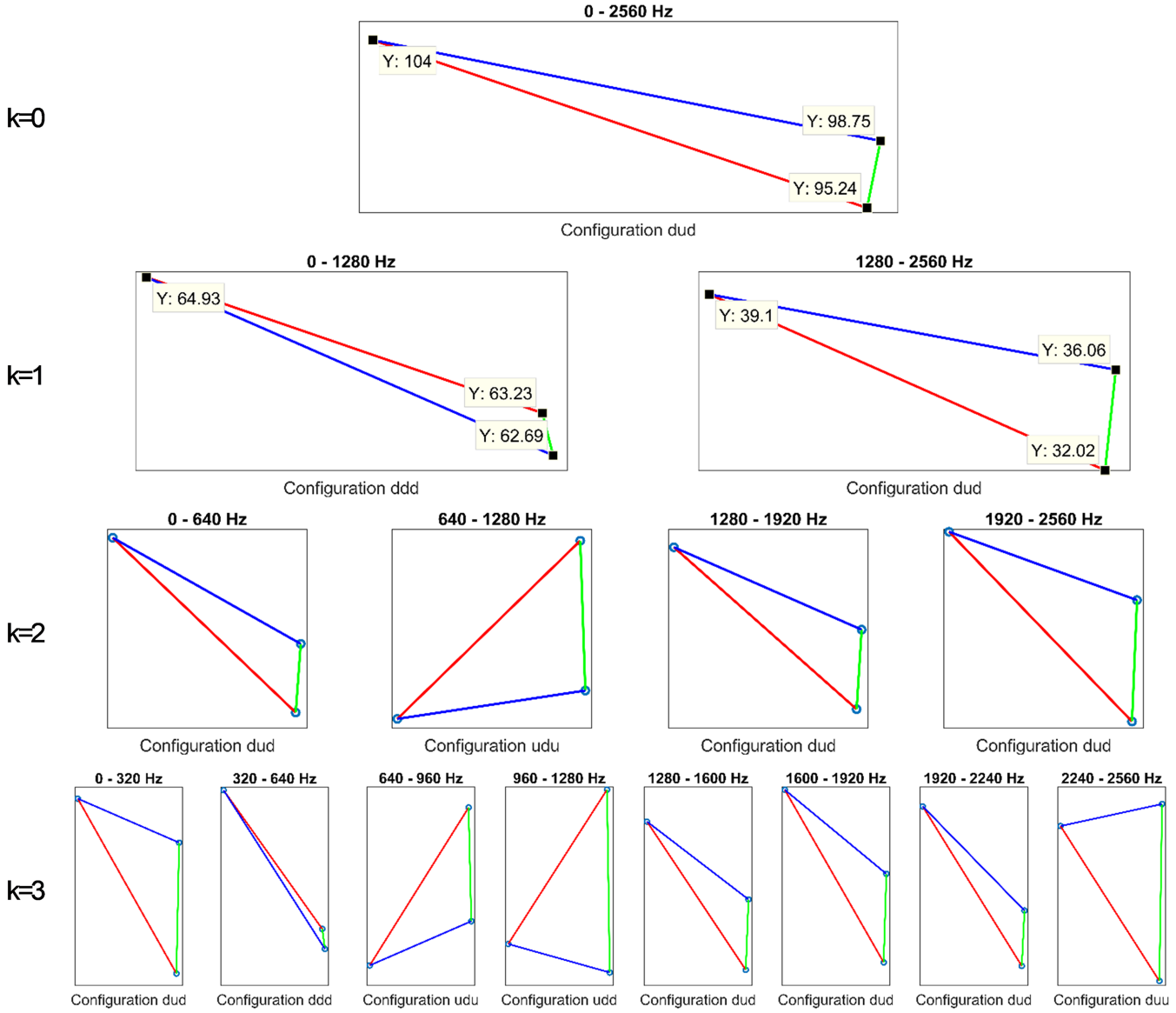

FIGURE 11 EGRSC of longitudinal accelerations

The first aspect to emphasize is the existence of large white areas in the ECBF with a threshold of 10%. Indeed, the first power packet of decomposition levels $k = 0$–3 is colored in white, as well as other power packets of decomposition level $k = 4$–7.

If we compute the spectral power variation from data shown in Figure 11, we obtain −8.4% (B → A) and −5.0% (B → L) for $k = 0$ and −2.6% (B → A, packet 1), −3.4% (B → L, packet 1), −18.1% (B → A, packet 2), and −7.8% (B → L, packet 2) for $k = 1$. Therefore, the first power packet will be colored in white, and the second one will be colored in its corresponding color according to that stated in Section 2.

The number of discarded frequency regions is highly increased when the threshold level is set to 25%. Indeed, the majority of the ECBF is colored in white.

When focusing on ECBFs with thresholds of 0% and 10%, it is observed that the left half of the ECBF (0–1,300 Hz) presents large areas of warm colors. The frequency region between 700 and 1,300 Hz shows orange and red colors only. There is also a dark red area around 300 Hz that comprises decomposition levels $k = 4$–9 and means the power is increased from operating state B to A. Blue sections are located below 250 Hz and around 500 Hz. The right half comprises the frequency range between 1,300 and 2,560 Hz, where a predominance of cold colors is observed. Just a small red area appears around 2,400 Hz at decomposition levels higher than $k = 4$.

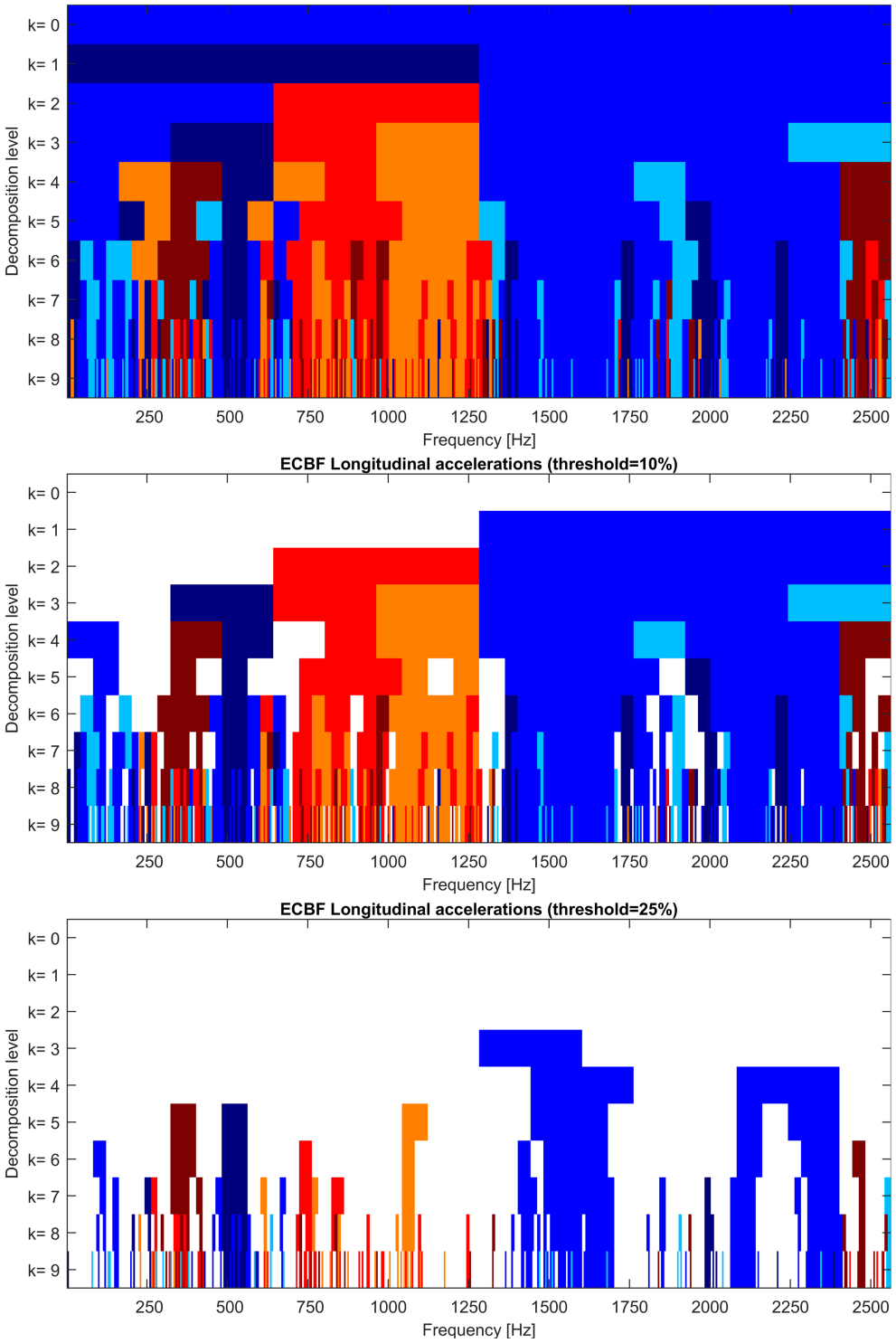

FIGURE 12 ECBF of longitudinal accelerations with three threshold levels: 0% (up), 10% (middle), and 25% (down)

The variable threshold allows selecting the frequency regions most sensitive to changes in the system. Four frequency regions with power reductions can be highlighted: 95–160, 455–570, 1,385–1,700, and 2,065–2,410 Hz. By looking at frequency regions with power increases, four frequency regions can be emphasized: 325–420, 715–860, and 1,045–1,105 Hz and a region around 2,500 Hz.

The white area corresponding to decomposition level $k = 0$ when any of the two thresholds is applied suggests that the vibrations recorded in the longitudinal direction are not very responsive to changes in the system. Deeper analysis also shows that the low-frequency range is less responsive than the high-frequency range. Anyhow, the frequency band

that corresponds to wheel corrugation experiences a power reduction, as should be expected after reprofiling the wheels. Besides, the power of packets containing the BSF and SPF is reduced after the maintenance, while the power of packets containing the BPFO and BPFI is increased.

4.3 | Lateral direction

Figure 13 illustrates the EGRSC of the lateral accelerations for decomposition levels $k = 0$, $k = 1$, $k = 2$, and $k = 3$. The EGRSC for decomposition level $k = 0$ shows a power reduction between states B and A and a further reduction between operating states B and L. This behavior corresponds to a "ddd" configuration and is one of the anticipated configurations after a repair of the system (see Section 2).

The first power packet of the decomposition level $k = 1$ presents a "ddd" configuration, whereas the second power packet differs from the first one and presents a "dud" configuration.

Decomposition level $k = 2$ gives four power packets. The first packet presents a "ddd" configuration, so the spectral power between 0 and 640 Hz is reduced always. The second power packet has an "udd" configuration, which means the power is increased between the operating states B and A, although the power level is lower at operating state L. The last two power packets (3 and 4) exhibit the "dud" configuration.

Eight power packets are obtained from the decomposition level $k = 3$. Four (power packets 1, 6, 7, and 8) of these packets present a "dud" configuration. This means that the spectral power is decreased between operating states B and A and B and L, while the spectral power rises between operating states A and L. Power packets 2 and 5 display a "ddd" configuration, which represents a continuous power reduction. The third power packet shows an "udd" configuration. In this case, the spectral power increases between the operating states B and A. Since then, it decreases and the final power is lower at operating state L than at B. The fourth power packet exhibits a "duu" configuration.

The ECBF corresponding to lateral accelerations is shown in Figure 14. Again, three threshold levels are set: 0% (no threshold), 10% and 25%.

Similarly to what happened in longitudinal vibrations, a lot of white areas are present in the ECBF when thresholds of 10% and 25% are selected. If we compute the spectral power variation from data shown in Figure 13, we obtain -11.85% (B $\rightarrow$ A) and -15.12% (B $\rightarrow$ L) for $k = 0$ and -4.6% (B $\rightarrow$ A, packet 1), -15.2% (B $\rightarrow$ L, packet 1), -25.6% (B $\rightarrow$ A, packet 2), and -14.9% (B $\rightarrow$ L, packet 2) for $k = 1$. Therefore, the first two rows of the ECBF with a threshold of 10% should be colored in blue, as it is done.

Discarded areas of ECBF (threshold 10%) comprise decomposition levels $k = 2$–9 and are located between 0 and 100 Hz, and between 600 and 1,500 Hz. The latter region varies its location as a function of the decomposition level. For $k = 2$–3, it is located between 640 and 1,280 Hz. For higher levels, the discarded area is established between 950 and 1,500 Hz. As it happened in the longitudinal vibrations, setting the threshold at 25% discards the majority of the area of the ECBF.

Taking into account the ECBFs with the three threshold levels, the frequency range between 1,500 and 2,560 Hz is mainly colored in blue with a few small regions in orange or red, regardless of the decomposition level and, even, the threshold value. The frequency region comprised between 0 and 1,500 Hz shows a diverse color combination. Alternating red/orange and blue stripes can be observed at decomposition levels higher than $k = 3$.

The variable threshold lets us choose the frequency regions most sensitive to the wheels reprofiling. Specifically, five interesting frequency regions with power reductions are located around 120, 250, 450–560, 1,525–1,700, and 1,765–2,400 Hz. By looking at frequency regions with power increases, three frequency regions can be highlighted at around 190, 350, and 645–790 Hz.

The frequency region that encompasses the wheel corrugation phenomenon experiences a spectral power reduction, which is consistent with the wheels reprofiling. The frequency region between 450 and 600 Hz must be underlined too. This region is colored in dark blue regardless of the decomposition level, which could suggest it responds very positively to maintenance actions.

5 | GENERAL OVERVIEW

By reviewing the most sensitive frequency regions of the three directions (vertical, longitudinal, and lateral), we can find the most sensitive frequency regions that are common to the three directions.

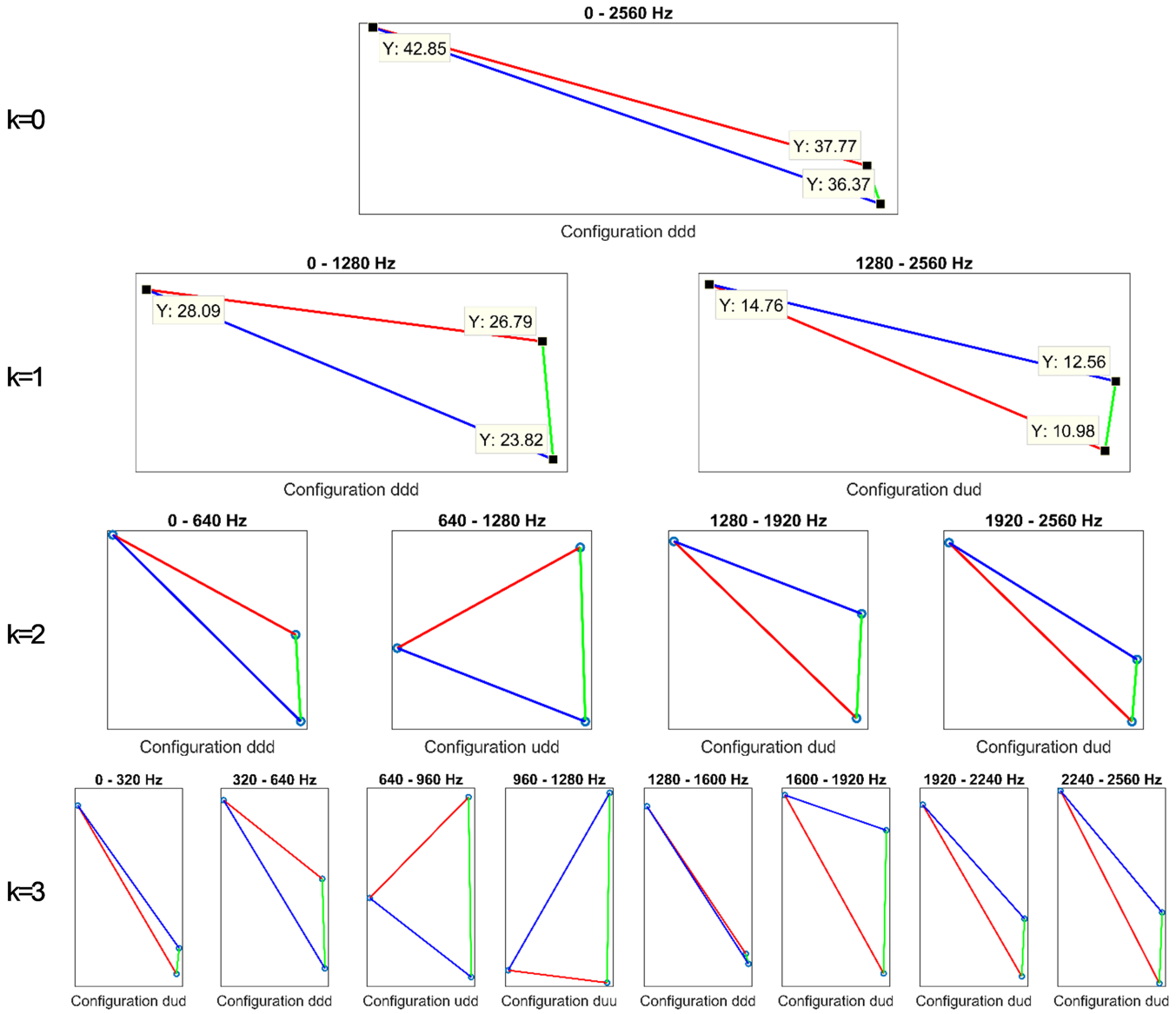

FIGURE 13 EGRSC of lateral accelerations

Of the most significant frequency regions, four have been identified that are common to all three directions. Three of these frequency regions present a power reduction, while the other shows a power increase.

The frequency regions with power reduction are located at 450–560, 1,500–1,700, and 1,800–2,400 Hz. The frequency region that increases its power is located at 600–800 Hz.

The performance of the high-frequency regions (above 1,280 Hz) is consistent with the effect of the wheels lathing. The frequency bands of 450–560 and 600–800 Hz seem to be related to the train-track interaction. The spectral power reduction observed in the 450–560 Hz band suggests that the excitation of this band is directly related to the condition of the wheel. However, the origin of vibrations in the 600- to 800-Hz frequency band could be other physical phenomena that were masked by the wheel corrugation. Hence, when the power of the other frequency regions is decreased significantly, it grows in this frequency band.

Finally, Table 5 summarizes the influence of the threshold value on the discarded areas of the ECBFs. The column "percentage of disregarded area" shows what percentage of the ECBF's whole surface is discarded. Because the surface of power packets or frequency regions varies according to the decomposition level, this value differs from the result of dividing the number of disregarded packets by 1,023 (the number of packets for $k = 9$).

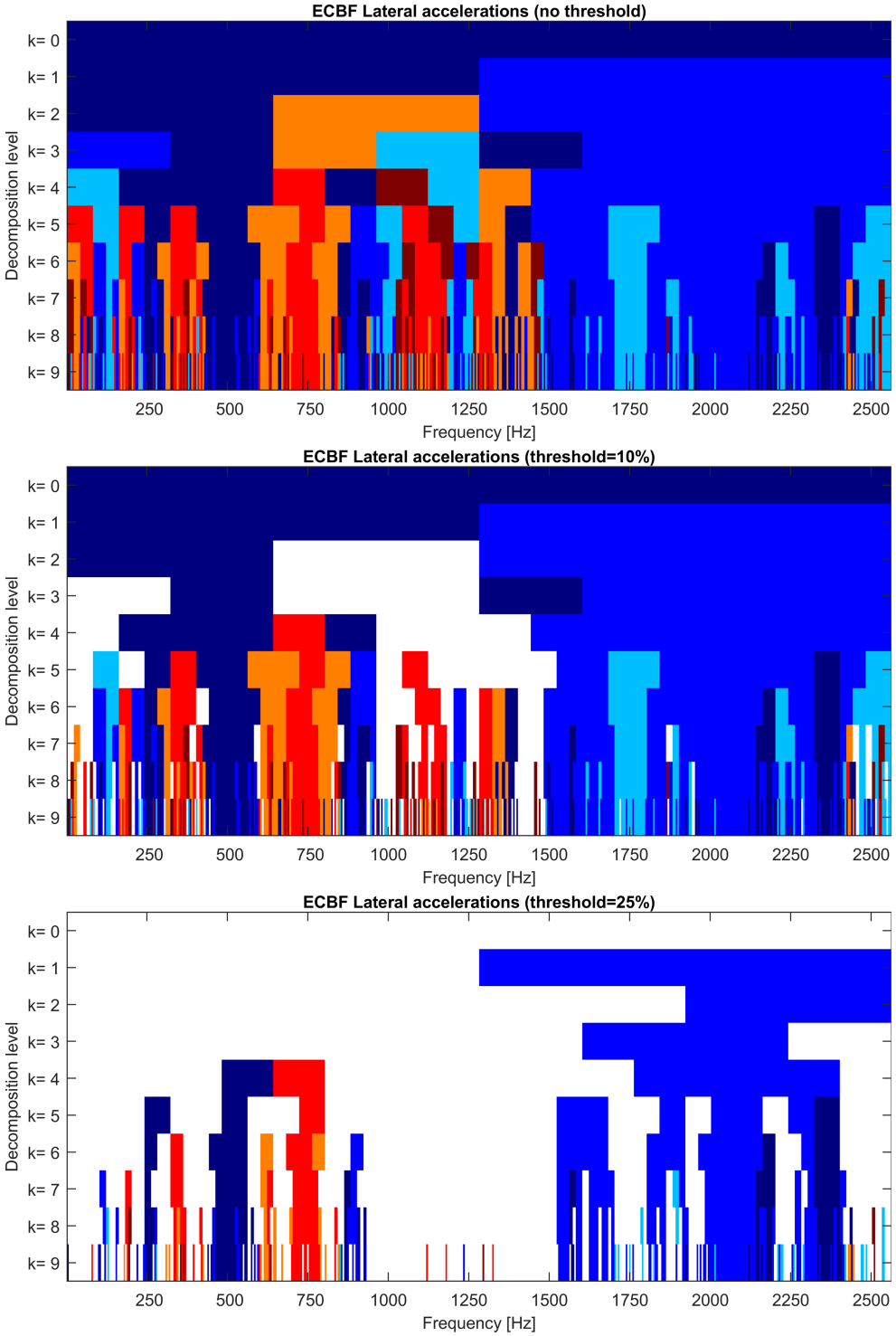

FIGURE 14 ECBF of lateral accelerations with three threshold levels: 0% (up), 10% (middle), and 25% (down)

Data in Table 5 show the vertical ECBF has the smallest number of disregarded packets and the lowest percentage of the disregarded area too. On the contrary, the longitudinal ECBF shows the largest number of disregarded packets and area.

It should be remembered that a packet colored in white (discarded) means the power variation of that packet is lower than the threshold. Thus, a large white area on the ECBF means the power of the packets is similar in the three operating states B, A, and L. Consequently, these packets are not very sensitive to changes in the system.

TABLE 5 Relation between the threshold and discarded packets

Direction	Threshold	Number of disregarded packets	Percentage of disregarded area
Longitudinal	0	0	0.00%
	10	139	28.83%
	25	607	78.01%
Lateral	0	0	0.00%
	10	161	17.50%
	25	583	66.41%
Vertical	0	0	0.00%
	10	79	9.88%
	25	433	46.88%

According to these data, vibrations measured in the vertical direction are the most sensitive to the maintenance action. If the original methods (GRSC and CBF) were used, minor variations (i.e., longitudinal vibrations) could be taken as significant and use those variations as an indicator of the condition of the train. As we saw, the wheels lathing has a small effect on the longitudinal vibrations, so it makes no sense its usage as an indicator of the operating condition.

6 | CONCLUSIONS

This paper presents an evolution of the GRSC and CBF methods, which implies a name change: EGRSC and ECBF.

The EGRSC uses a new and clearer nomenclature that separates the name of the state configurations from the state names. This new nomenclature uses a combination of three letters as previously, but the system is binary now: "d" (down) for negative slopes and "u" (up) for positive slopes.

A new color code is defined in the ECBF, and a variable threshold is introduced. This threshold sets a value (relative to the power of the operating state B) to discard the power packets whose power variation is lower than that threshold. The discarded power packets are colored in white in the ECBF.

The EGRSC and ECBF are used in the vibratory study of a HST bogie. Each EGRSC and ECBF collects information from thousands of vibration signals and displays that information intuitively and understandably.

The HST bogie is studied before and after a major maintenance operation that consisted of reprofiling the wheels. For that purpose, accelerometers are installed on the axle box cover of a trailer axle, in the three space directions.

Taking into account the results of EGRSC and ECBF methods, it can be established that the wheels reprofiling improved the dynamic performance of the bogie, as a lower vibration level is recorded. This phenomenon is observed in all directions.

The new threshold of the ECBF also allows identifying the most and less responsive vibration directions to wheel reprofiling. Data show that the wheel reprofiling affects especially the vertical vibrations, so these vibrations should be taken as main indicators of the bogie condition.

It has been observed a vibration-level reduction in the frequency range 1,500 to 2,400 Hz, which corresponds to the wheel corrugation after the maintenance operation. This effect is observed in the three space directions when considering low decomposition levels. A spectral power reduction is also noted in the power packets that contain the BSF and SPF.

Finally, a detailed analysis through EGRSC and ECBF focused on medium and higher decomposition levels shows the existence of particular frequency regions with the same performance in the three directions of space: the spectral power decreases significantly in the frequency ranges: 450–550, 1,500–1,700, and 1,800–2,400 Hz. Additionally, the spectral power is significantly raised in the 600- to 800-Hz frequency range. These four frequency bands should be used as indicators of the bogie condition on future maintenance actions.

ACKNOWLEDGMENTS

The research work described in this paper was supported by the Spanish Government through the MAQ-STATUS DPI2015-69325-C2-1-R project and by the UNED through UNED 2021-MEC-25 project.

CONFLICT OF INTERESTS

The authors declare no conflict of interest.

DATA AVAILABILITY STATEMENT

Data subject to third party restrictions.

ORCID

Alejandro Bustos https://orcid.org/0000-0001-7513-6058
Higinio Rubio https://orcid.org/0000-0001-6122-3011
Cristina Castejon https://orcid.org/0000-0002-5823-7372
Juan Carlos Garcia-Prada https://orcid.org/0000-0002-7793-8625

REFERENCES

1. Union Internationale des Chemins de fer (UIC). High speed lines in the world. 2019. https://uic.org/IMG/pdf/20190328_high_speed_lines_in_the_world.pdf
2. Union Internationale des Chemins de fer (UIC). High speed traffic in the world. 2019. https://uic.org/IMG/pdf/20190122_high_speed_passenger_km.pdf
3. Esslinger V, Kieselbach R, Koller R, Weisse B. The railway accident of Eschede – technical background. *Eng Fail Anal*. 2004;11(4):515-535. https://doi.org/10.1016/j.engfailanal.2003.11.001
4. Railway Gazette International. Design flaws and poor management caused Wenzhou collision, report confirms. 2012. Accessed July 18, 2019. https://www.railwaygazette.com/news/single-view/view/design-flaws-and-poor-management-caused-wenzhou-collision-report-confirms.html
5. Antipov AG, Markov AA. 3D simulation and experiment on high speed rail MFL inspection. *NDT E Int*. 2018;98:177-185. https://doi.org/10.1016/j.ndteint.2018.04.011
6. Matsumoto A, Sato Y, Ohno H, et al. Actual states of wheel/rail contact forces and friction on sharp curves–Continuous monitoring from in-service trains and numerical simulations. *Wear*. 2014;314(1-2):189-197. https://doi.org/10.1016/j.wear.2013.11.046
7. Cavuto A, Martarelli M, Pandarese G, Revel GM, Tomasini EP. Train wheel diagnostics by laser ultrasonics. *Measurement*. 2016;80:99-107. https://doi.org/10.1016/j.measurement.2015.11.014
8. Li D, Kuang KSC, Koh CG. Rail crack monitoring based on Tsallis synchrosqueezed wavelet entropy of acoustic emission signals: A field study. *Struct Health Monit*. 2018;17(6):1410-1424. https://doi.org/10.1177/1475921717742339
9. Frankenstein B, Hentschel D, Pridoehl E, Schubert F. Hollow shaft integrated health monitoring system for railroad wheels. Proc. SPIE 5770, Advanced Sensor Technologies for Nondestructive Evaluation and Structural Health Monitoring. 2005:46–55. https://doi.org/10.1117/12.602310
10. Lunys O, Dailydka S, Bureika G. Investigation on features and tendencies of axle-box heating. *Transp Probl*. 2017; 10(1):105-114. https://doi.org/10.21307/tp-2015-011
11. Alemi A, Corman F, Lodewijks G. Condition monitoring approaches for the detection of railway wheel defects. *Proc Inst Mech Eng Part F J Rail Rapid Transit*. 2017;231(8):961-981. https://doi.org/10.1177/0954409716656218
12. Jemec V. Evaluation of defects and cracks in carriage axles using non-destructive testing. *Int Conf Part Eur NDT Days Prague Nov 2007 NDE Saf 2007*. 2007;107-118.
13. Gomez E, Giménez JG, Alonso A. Method for the reduction of measurement errors associated to the wheel rotation in railway dynamometric wheelsets. *Mech Syst Signal Process*. 2011;25(8):3062-3077. https://doi.org/10.1016/j.ymssp.2011.05.006
14. Li C, Luo S, Cole C, Spiryagin M. An overview: modern techniques for railway vehicle on-board health monitoring systems. *Veh Syst Dyn*. 2017;55(7):1045-1070. https://doi.org/10.1080/00423114.2017.1296963
15. Zhou L, Brunskill HP, Lewis R. Real-time non-invasive measurement and monitoring of wheel–rail contact using ultrasonic reflectometry. *Struct Health Monit*. 2019;18(5-6):1953-1965. http://dx.doi.org/10.1177/1475921719829882
16. Chong SY, Lee J-R, Shin H-J. A review of health and operation monitoring technologies for trains. *Smart Struct Syst*. 2010;6(9):1079-1105. https://doi.org/10.12989/sss.2010.6.9.1079
17. Randall RB. *Vibration-Based Condition Monitoring: Industrial, Aerospace and Automotive Applications*. John Wiley & Sons, Ltd; 2010.
18. Pennacchi P, Chatterton S, Vania A, Ricci R, Borghesani P. Experimental evidences in bearing diagnostics for traction system of high speed trains. 2013 *Progn Health Manag Conf (Phm)*. 33:739-744. http://www.aidic.it/cet/13/33/124.pdf
19. Yi C, Lin J, Zhang W, Ding J. Faults Diagnostics of Railway Axle Bearings Based on IMF's Confidence Index Algorithm for Ensemble EMD. *Sensors*. 2015;15(5):10991-11011. https://doi.org/10.3390/s150510991
20. Li Y, Liang X, Chen Y, Chen Z, Lin J. Wheelset bearing fault detection using morphological signal and image analysis. *Struct Control Health Monit*. 2020;27(11). https://doi.org/10.1002/stc.2619
21. Li Z, Wei L, Dai H, Zeng Y, Wang Y. Identification method of wheel flat based on Hilbert-Huang transform. *J Traffic Trans Eng*. 2012;12(4):33-41.
22. Li Y, Zuo MJ, Lin J, Liu J. Fault detection method for railway wheel flat using an adaptive multiscale morphological filter. *Mech Syst Signal Process*. 2017;84:642-658. https://doi.org/10.1016/j.ymssp.2016.07.009

23. Jia S, Dhanasekar M. Detection of rail wheel flats using wavelet approaches. *Struct Health Monit Int J*. 2007;6(2):121-131. https://doi.org/10.1177/1475921706072066
24. Hassan M, Bruni S. Experimental and numerical investigation of the possibilities for the structural health monitoring of railway axles based on acceleration measurements. *Struct Health Monit*. 2019;18(3):902-919. http://dx.doi.org/10.1177/1475921718786427
25. Rolek P, Bruni S, Carboni M. Condition monitoring of railway axles based on low frequency vibrations. *Int J Fatigue*. 2016;86:88-97. https://doi.org/10.1016/j.ijfatigue.2015.07.004
26. Gómez MJ, Corral E, Castejón C, García-Prada J. Effective Crack Detection in Railway Axles Using Vibration Signals and WPT Energy. *Sensors*. 2018;18(5):1603. https://doi.org/10.3390/s18051603
27. Li F, Sun X, Qiu J, Zhou L, Li H, Meng G. Guided wave propagation in high-speed train axle and damage detection based on wave mode conversion. *Struct Control Health Monit*. 2015;22(9):1133-1147. https://doi.org/10.1002/stc.1739
28. Qiu J, Li F, Wang J. Damage detection for high-speed train axle based on the propagation characteristics of guided waves: damage detection in high-speed train axle based on GWs. *Struct Control Health Monit*. 2017;24(3):e1891. https://doi.org/10.1002/stc.1891
29. Papaelias M, Amini A, Huang Z, Vallely P, Dias DC, Kerkyras S. Online condition monitoring of rolling stock wheels and axle bearings. *Proc Inst Mech Eng Part F J Rail Rapid Transit*. 2016;230(3):709-723. https://doi.org/10.1177/0954409714559758
30. Bustos A, Rubio H, Castejón C, García-Prada J. EMD-Based Methodology for the Identification of a High-Speed Train Running in a Gear Operating State. *Sensors*. 2018;18(3):793. https://doi.org/10.3390/s18030793
31. Ham YS. Evaluation of Running Safety for Railway vehicles Based on Vibration Acceleration of Bogie. *Key Eng Mater*. 2014;625:689-694. https://doi.org/10.4028/www.scientific.net/KEM.625.689
32. Wang J, Song C, Wu P, Dai H. Wheel reprofiling interval optimization based on dynamic behavior evolution for high speed trains. *Wear*. 2016;366-367:316-324. https://doi.org/10.1016/j.wear.2016.06.016
33. Gasparetto L, Alfi S, Bruni S. Data-driven condition-based monitoring of high-speed railway bogies. *Int J Rail Transp*. 2013;1(1-2):42-56. https://doi.org/10.1080/23248378.2013.790137
34. Zhang L-H, Wang Y-W, Ni Y-Q, Lai S-K. Online condition assessment of high-speed trains based on Bayesian forecasting approach and time series analysis. *Smart Struct Syst*. 2018;21(5):705-713. https://doi.org/10.12989/sss.2018.21.5.705
35. Wang YW, Ni YQ, Wang X. Real-time defect detection of high-speed train wheels by using Bayesian forecasting and dynamic model. *Mech Syst Signal Process*. 2020;139:106654. https://doi.org/10.1016/j.ymssp.2020.106654
36. Bustos A, Rubio H, Castejon C, Garcia-Prada JC. Condition monitoring of critical mechanical elements through Graphical Representation of State Configurations and Chromogram of Bands of Frequency. *Measurement*. 2019;135:71-82. https://doi.org/10.1016/j.measurement.2018.11.029
37. Braun S, Ewins DJ, Rao SS. *Encyclopedia of Vibration*. Academic Press; 2002.
38. Norton MP, Karczub DG. *Fundamentals of Noise and Vibration Analysis for Engineers*. 2nd edition. Cambridge Univ Press. 2003. https://doi.org/10.1017/CBO9781139163927
39. Kouroussis G, Connolly DP, Verlinden O. Railway-induced ground vibrations—a review of vehicle effects. *Int J Rail Transp*. 2014;2(2):69-110. https://doi.org/10.1080/23248378.2014.897791

How to cite this article: Bustos A, Rubio H, Castejon C, Garcia-Prada JC. Enhancement of chromatographic spectral technique applied to a high-speed train. *Struct Control Health Monit*. 2021;28(12):e2842. doi: 10.1002/stc.2842